J. Fluid Mech. (1991), *vol.* 224, *pp.* 361–382
Printed in Great Britain

On the baroclinic instability of cold-core coupled density fronts on a sloping continental shelf

By GORDON E. SWATERS

Applied Mathematics Institute, Department of Mathematics *and* Institute of Earth and Planetary Physics, University of Alberta, Edmonton, Alberta, Canada T6G 2G1

(Received 27 March 1990 and in revised form 27 August 1990)

A theory is presented to describe the linear *baroclinic* instability of coupled density fronts on a sloping continental shelf. The new baroclinic model equations used to study the instability process correspond to an 'intermediate lengthscale' dynamical balance. Specifically, the frontal dynamics, while geostrophic, is not quasi-geostrophic because frontal height deflections are not small in comparison with the frontal scale height. The evolution of the frontal height is strongly coupled to the geostrophic pressure in the surrounding slope water through the hydrostatic balance which expresses the continuity of the dynamic pressures across the frontal interface. The deeper surrounding slope water evolves quasi-geostrophically and is coupled to the front by baroclinic vortex-tube stretching/compression associated with the perturbed density front (allowing the release of mean frontal potential energy) and the topographic vorticity gradient associated with the sloping bottom. It is shown that the baroclinic stability characteristics are principally determined by a so-called non-dimensional *interaction* parameter (denoted μ) which physically measures the ratio of the destabilizing baroclinic vortex-tube stretching/compression to the stabilizing topographic vorticity gradient. For a given along-front mode wavenumber it is shown that a minimum μ is required for instability. Several other general stability results are presented: necessary conditions for instability, growth rate and phase speed bounds, the existence of a high wavenumber cutoff, and a semicircle theorem for the unstable modes. The linear stability equations are solved exactly for a parabolic coupled density front and a detailed description of the spatial and temporal characteristics of the instabilities is given. For physically realistic parameter values the instabilities are manifested as amplifying topographic Rossby waves in the slope water, and on the density front the unstable perturbations take the form of amplifying anticyclones which have maximum amplitude on the offshore side.

1. Introduction

When dense water is formed at the surface or otherwise released in a shallow sea such as the slope water on a continental shelf it may reach the bottom and form a bottom vein or mesoscale gravity current. If the bottom is sloping, then the combined influences of the Coriolis and buoyancy stresses may force the current to be transversely constrained and flow with the coastline to its right (oriented relative to the direction of flow). Examples include the Denmark Strait overflow (Smith 1976), Antarctic Bottom Water formed in the Weddell Sea (Whitehead & Worthington 1982), deep water formation in the Adriatic Sea (Zoccolotti & Salusti

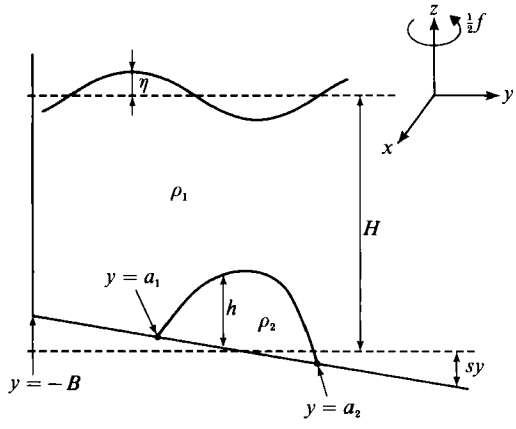

FIGURE 1. Geometry of the two-layer model used in this paper.

1987) and the elongated cool pool which forms and flows on the Mid-Atlantic Bight (Houghton *et al.* 1982), among others. These currents play an important role in the mesoscale physical and biological dynamics of the benthic boundary layer on a shelf slope (e.g. Cooper 1955; Johnson & Schneider 1969). In particular, it is possible that the formation of bottom-trapped cold-core isolated eddies on continental shelves (e.g. Armi & D'Asaro 1980; Houghton *et al.* 1982; Mory, Stern & Griffiths 1987 and Nof 1983; among others) is the result of the instability of these currents. The principal objective of this paper is to present an 'intermediate lengthscale' (in the sense of Charney & Flierl 1981) theory to describe the baroclinic instability of a dense gravity current on a sloping continental shelf.

There have been relatively few analytical studies of the stability characteristics of dense gravity currents because of the complexity associated with retaining the ageostrophic terms in the momentum equations and the space–time density gradients in the mass conservation equation. The density configuration for these currents will generally contain isopcynals which intersect the bottom on either side of the flow (see figure 1). The stratification characteristics of these currents will therefore resemble a bottom-trapped coupled density front. Because the isopcynal deflections associated with these currents are large in comparison to the scale height of the current it is not possible to neglect the space and time derivatives of the current height in comparison to the horizontal divergence terms in the continuity equation. Consequently, a quasi-geostrophic theory is unlikely to be able to describe the dynamics of these fronts. Notwithstanding this latter point, Smith (1976) was able to apply a two-layer quasi-geostrophic model to describe some aspects of the baroclinic instability found in the Denmark Strait overflow during August–September 1973.

Much of the recent theoretical work on the stability of coupled density fronts is based on the study by Griffiths, Killworth & Stern (1982, hereinafter referred to as GKS). This study presented a long-wavelength perturbation analysis of the ageostrophic barotropic instability of a gravity current on a sloping bottom. (GKS also studied finite wavenumbers.) In order to focus attention on barotropic instability processes (i.e. the release of mean kinetic energy), GKS worked with a reduced-gravity single-layer theory in which the overlying fluid was infinitely deep and motionless. The instability was the result of a coupling of the two free lateral

boundary streamlines and did not require, as in quasi-geostrophic theory (see Pedlosky 1987, §7.14 or LeBlond & Mysak 1978, §44), a zero in the cross-shelf potential vorticity gradient. While the instability was primarily barotropic, the unstable mode described by GKS necessarily had a concomitant release of mean potential energy. In general, the coupled front was found to be quite unstable when the width of the current was of the same scale as the Rossby deformation radius.

When GKS compared the predictions of their theory to laboratory simulations of the instability of a buoyant coupled density front substantial differences were found. For example, the unstable modes described by GKS have asymptotically small along-front wavenumbers while the observed instabilities occurred over a range of wavenumbers including those corresponding to finite wavelengths. Another difficulty with the theory was that the observed instability had a dominant lengthscale independent of the current width in contradiction to the theoretical prediction. These differences were attributed to the presence of another, possibly baroclinic, unstable mode outside the range of applicability of the GKS analysis.

Paldor & Killworth (1987) adapted the GKS analysis to study the long-wavelength instability of a surface or warm-core coupled front in a two-layer f-plane model. Two unstable modes were found. One of these modes is a baroclinically modified form of the GKS barotropic mode and the other mode is similar to the unstable mode found by Killworth, Paldor & Stern (1984) for a baroclinic isolated front. Killworth & Stern (1982) applied the GKS theory to describe the ageostrophic instability of a surface coastal density current in a barotropic, flat-bottomed f-plane model. Their results showed that a necessary condition for the current to be unstable was that the mean potential vorticity increased in the onshore direction. Here again, the instability, while barotropic, did not require an extremum in the mean potential vorticity. The theory developed in this paper focuses not on the barotropic energy conversion mechanism described above, but rather on the baroclinic instability transfer of mean potential energy to perturbation kinetic energy.

The model equations that we use to study the baroclinic instability process will correspond to strongly interacting hybrid 'quasi-geostrophic, intermediate-lengthscale geostrophic dynamics' (see Charney & Flierl 1981). Specifically, the dynamics of the surrounding much deeper slope water is assumed to be quasi-geostrophic but the dynamics of the coupled density front, while geostrophic, is of course not quasi-geostrophic because deflections in the current thickness are not small in comparison with the scale height of the front itself. This balance represents a middle dynamical regime between a more complete ageostrophic balance and the lower-frequency/wavenumber quasi-geostrophic balance (see also Cushman-Roisin 1986). As a result, while the velocity fields in both the gravity-current interior and surrounding slope water will be geostrophically determined (but not uncoupled), the dynamical evolution of the height of the coupled density front will be strongly coupled to the geostrophic pressure field in the surrounding slope water. This model, which is presented in §2, is derived in a formal asymptotic expansion based on two-layer shallow-water theory assuming a small (appropriately scaled) shelf slope parameter. The dynamical balance described here has been used to model the dynamics of ventilated coherent cold eddies on a sloping bottom (Swaters & Flierl 1991).

A major result of our analysis will be to show in §3 that the stability characteristics are determined in large part by a so-called 'interaction' parameter (denoted μ) which physically measures the ratio of induced baroclinic vortex-tube stretching/compression in the surrounding slope water (resulting from the perturbed density

front) to the stabilizing vorticity gradient associated with the sloping bottom (which acts as a topographic beta-plane in the dynamics of the slope water). We shall show that for a given along-front wavenumber, a minimum μ is required for baroclinic instability.

Several other general stability characteristics will be shown in §3: growth rate and phase speed bounds, the existence of a high-wavenumber cutoff, a semicircle theorem and a minimum interaction condition. We are also able to provide a simple linear stability criterion for arbitrary disturbances. In addition, we shall show that associated with the instability is a net onshore flux of perturbation heat or, equivalently, a net offshore flux of relatively cool temperature anomalies in the slope water. Finally, we would like to comment that the analysis to be presented here has other applications. For example, it will be easy to see how this analysis can be applied to study the baroclinic instability of warm-core or surface coupled fronts on a *planetary* beta-plane.

In §4 we illustrate our theoretical work with the analytical solution that can be obtained for a simple parabolic coupled density front. Concluding remarks and a summary are given in §5.

2. Formulation of the baroclinic model

The basic model we assume is an f-plane two-layer system (both layers are assumed hydrostatic, homogeneous and incompressible) with a linearly varying bottom slope (see figure 1). Since the derivation of the model equations has been presented elsewhere (Swaters & Flierl 1991; Whitehead *et al.* 1990), our presentation here will be relatively brief. The non-dimensional equations for the slope water (layer 1) are given by

$$s\boldsymbol{u}_{1_t} + \delta(\boldsymbol{u}_1 \cdot \boldsymbol{\nabla})\,\boldsymbol{u}_1 + \hat{\boldsymbol{e}}_3 \times \boldsymbol{u}_1 + \boldsymbol{\nabla}\eta = \boldsymbol{0}, \tag{2.1a}$$

$$sh_t + \boldsymbol{\nabla}\cdot[\boldsymbol{u}_1(\delta h - sy - 1)] = 0, \tag{2.1b}$$

and the non-dimensional equations for the double density front (layer 2) are given by

$$s\boldsymbol{u}_{2_t} + s(\boldsymbol{u}_2 \cdot \boldsymbol{\nabla})\,\boldsymbol{u}_2 + \hat{\boldsymbol{e}}_3 \times \boldsymbol{u}_2 + \boldsymbol{\nabla}p = \boldsymbol{0}, \tag{2.2a}$$

$$h_t + \boldsymbol{\nabla}\cdot(h\boldsymbol{u}_2) = 0. \tag{2.2b}$$

The requirement that the pressure be continuous across the front–slope interface is given by

$$\delta\eta + \delta h - s(y+p) = 0. \tag{2.3}$$

The coordinates are (x, y) and t is time. Subscripts with respect to x, y and t indicate partial differentiation, and $\boldsymbol{\nabla} = (\partial_x, \partial_y)$. The scaled slope parameter s is given by $s = s^*L/H$, where s^*, L and H are the unscaled slope parameter, horizontal lengthscale and mean height of layer 1 above the front, respectively. The parameter $\delta = h_0/H$, where h_0 is a representative scale for the undisturbed height of the front above the sloping topography. In order to focus attention on the baroclinic problem we have neglected terms of $O(g'\eta/g)$ in (2.1b) and (2.3), where the reduced gravity is given by $g' = g(\rho_2 - \rho_1)/\rho_2 > 0$ (stable stratification) and g is the gravitational acceleration.

The following boundary conditions are imposed on the model. Suppose the projection on the plane $z = 0$ of a particular intersection of the front with the sloping bottom is given by $\phi(x, y, t) = 0$. The kinematic condition is given by

$$\phi_t + \boldsymbol{u}_2 \cdot \boldsymbol{\nabla}\phi = 0 \quad \text{on} \quad \phi(x, y, t) = 0. \tag{2.4}$$

And the frontal thickness satisfies

$$h(x, y, t) = 0 \quad \text{on} \quad \phi(x, y, t) = 0. \tag{2.5}$$

The non-dimensional location of the coast is given by $y = -B$. On the coast we require that there be no normal flow in the slope water, i.e.

$$v_1(x, -B, t) = 0. \tag{2.6}$$

In the offshore direction (i.e. $y \to \infty$) we shall require that the slope-water velocity be bounded.

It has been argued (e.g. Mory *et al.* 1987; Nof 1983; GKS; among others) that the formation of isolated cold eddies on a sloping bottom may be the result of the instability of bottom-trapped coupled density fronts. With this possible application in mind we shall estimate the non-dimensional parameters δ and s based on oceanographic observations of isolated cold eddies on a sloping bottom. For example, the observations of the cold pool reported by Houghton *et al.* (1982) correspond to approximate parameter values of $s^* \approx 1.2$ m/km, $h_0 \approx 40$ m and $H \approx 250$ m suggesting $s \approx 7 \times 10^{-2}$, and $\delta \approx 1.6 \times 10^{-1}$. These parameter values also suggest $L \approx 15$ km (for midlatitudes) and an *advective* timescale of about $T = fL/(g's^*) \approx 7$ days. As a rough first approximation, we see that $s \approx \delta \approx O(10^{-1})$ and consequently that the ageostrophic terms in the interior frontal momentum balance are at least an order of magnitude smaller than the derivatives of $h(x, y, t)$ in the front continuity equation. The scalings suggest that we set

$$\delta = \mu s, \tag{2.7}$$

where $\mu \approx O(1)$. For the above parameter estimates it follows that $\mu \approx 2$.

Substitution of (2.7) into (2.1) and (2.3) yields the following set of equations for the coupled front and surrounding slope-water problem:

$$\hat{\boldsymbol{e}}_3 \times \boldsymbol{u}_1 + \nabla\eta = -s\boldsymbol{u}_{1_t} - s\mu(\boldsymbol{u}_1 \cdot \nabla)\boldsymbol{u}_1, \tag{2.8a}$$

$$\nabla \cdot \boldsymbol{u}_1 = sh_t - s\nabla \cdot (y\boldsymbol{u}_1) + \mu s\nabla \cdot (h\boldsymbol{u}_1), \tag{2.8b}$$

$$\hat{\boldsymbol{e}}_3 \times \boldsymbol{u}_2 - \hat{\boldsymbol{e}}_2 + \mu\nabla(h + \eta) = -s\boldsymbol{u}_{2_t} - s(\boldsymbol{u}_2 \cdot \nabla)\boldsymbol{u}_2, \tag{2.9a}$$

$$h_t + \nabla \cdot (h\boldsymbol{u}_2) = 0. \tag{2.9b}$$

The front boundary conditions remain unchanged. The location of the slope parameter s in (2.8a, b) occurs in such a way that to $O(s)$ the dynamics of the shelf water will be quasi-geostrophic. The location of the slope parameter s in (2.9a, b) implies that the interior frontal dynamics is essentially geostrophic but not quasi-geostrophic since changes in h are comparable with h itself.

We can exploit the fact that $0 < s \ll 1$ by constructing a straightforward asymptotic expansion of the form

$$(\eta, p, \boldsymbol{u}_1, \boldsymbol{u}_2, h, \phi) \sim (\eta_0, p_0, \boldsymbol{u}_{10}, \boldsymbol{u}_{20}, h_0, \phi_0) + s(\eta_1, p_1, \boldsymbol{u}_{11}, \boldsymbol{u}_{21}, h_1, \phi_1) + \ldots.$$

Substitution of this expansion into (2.4), (2.5), (2.8) and (2.9) yields the $O(1)$ problem in the form (see Swaters & Flierl 1991)

$$(\nabla^2\partial_t - \partial_x)\eta_0 - h_{0_x} + \mu J(\eta_0, \nabla^2\eta_0) = 0, \tag{2.10a}$$

$$h_{0_t} + h_{0_x} + \mu J(\eta_0, h_0) = 0, \tag{2.10b}$$

with the auxiliary $O(1)$ relations

$$\boldsymbol{u}_{10} = \hat{\boldsymbol{e}}_3 \times \boldsymbol{\nabla}\eta_0, \tag{2.11a}$$

$$\boldsymbol{u}_{20} = \hat{\boldsymbol{e}}_1 + \mu\hat{\boldsymbol{e}}_3 \times \boldsymbol{\nabla}(\eta_0 + h_0), \tag{2.11b}$$

$$p_0 = -y + \mu(\eta_0 + h_0), \tag{2.11c}$$

and the frontal free-boundary conditions

$$\left.\begin{aligned} \phi_{0_t} + \phi_{0_x} + \mu J(\eta_0 + h_0, \phi_0) = 0, \\ h_0 = 0, \end{aligned}\right\} \quad \text{on} \quad \phi_0 = 0, \tag{2.12a, 2.12b}$$

where the Jacobian is given by $J(A, B) = A_x B_y - A_y B_x$ and where $\nabla^2 = \partial^2/\partial x^2 + \partial^2/\partial y^2$. The no-normal-flow condition on the coast for the slope water is given by

$$\eta_{0_x} = 0 \quad \text{on} \quad y = -B, \tag{2.13}$$

and the offshore boundary condition for the slope water is given by

$$|\eta_0| \quad \text{remains bounded as} \quad y \to \infty. \tag{2.14}$$

For notational convenience we shall henceforth delete the zero subscript on these $O(1)$ fields.

The model (2.10)–(2.14) has an exact nonlinear along-shelf solution in the form

$$\eta = \eta_0(y) = -\int_0^y U_0(\xi)\,\mathrm{d}\xi \quad \text{for} \quad -B < y < \infty, \tag{2.15a}$$

$$h = h_0(y) \quad \text{for} \quad a_1 < y < a_2, \tag{2.15b}$$

with the boundaries of the coupled front given by

$$\phi = \begin{cases} \phi_1 = y - a_1, & (2.16a) \\ \phi_2 = y - a_2, & (2.16b) \end{cases}$$

where it is assumed that $-B < a_1 < a_2$ and $h_0(a_1) = h_0(a_2) = 0$ (see figure 1).

3. Linear stability problem and general stability characteristics

3.1. *Linear stability equations and boundary conditions*

In order to derive the stability equations we assume that

$$h = h_0(y) + h'(x, y, t), \tag{3.1a}$$

$$\eta = \eta_0(y) + \eta'(x, y, t), \tag{3.1b}$$

$$\phi = \begin{cases} \phi_1 = y - a_1 - \phi_1'(x, t), & (3.2a) \\ \phi_2 = y - a_2 - \phi_2'(x, t), & (3.2b) \end{cases}$$

and substitute into the model equations (2.10)–(2.14) and linearize about $h_0(y)$ and $\eta_0(y)$.

In the region $a_1 < y < a_2$ the linearized equations take the form (after dropping the prime notation for the perturbation fields)

$$[\partial_t + \mu U_0(y)\,\partial_x]\nabla^2\eta - (1 + \mu U_{0_{yy}})\,\eta_x - h_x = 0, \tag{3.3a}$$

$$[\partial_t + (\mu U_0 + 1)\,\partial_x]\,h + \mu h_{0_y}\,\eta_x = 0. \tag{3.3b}$$

In the non-frontal regions $-B < y < a_1$ and $y > a_2$ the stability problem for the slope water is given by

$$[\partial_t + \mu U_0(y)\,\partial_x]\nabla^2\eta - (1+\mu U_{0_{yy}})\,\eta_x = 0. \tag{3.3c}$$

The linearized and Taylor-expanded boundary conditions are given by

$$h + h_{0_y}\phi_{1,2} = 0 \quad \text{on} \quad y = a_{1,2}, \tag{3.4a, b}$$

$$\phi_{1,2_t} + (1+\mu U_0 - \mu h_{0_y})\,\phi_{1,2_x} - \mu(\eta+h)_x = 0 \quad \text{on} \quad y = a_{1,2}, \tag{3.4c, d}$$

$$\eta_x = 0 \quad \text{on} \quad y = -B, \tag{3.4e}$$

$$|\eta| \text{ remains bounded as } y \to \infty. \tag{3.4f}$$

There must also be continuity conditions on the slope-water pressure and normal mass flux across $y = a_1$ and $y = a_2$ and at any other points where U_0 and U_{0_y} are discontinuous.

3.2. *Perturbation energetics*

Before turning to the derivation of the normal-mode equations, we want to obtain necessary conditions for instability from the energy equation associated with (3.3). If (3.3*a*) and (3.3*c*) are multiplied by $\eta(x,y,t)$ and subsequently integrated over $-B < y < \infty$ and $0 < x < \lambda$, where λ is the along-shelf wavelength of the perturbation, it follows that

$$\frac{\partial}{\partial t}\int_{-B}^{\infty}\langle\nabla\eta\cdot\nabla\eta\rangle\,\mathrm{d}y = 2\int_{-B}^{\infty}\tau U_{0_y}\,\mathrm{d}y + 2\int_{a_1}^{a_2}\langle v_1 h\rangle\,\mathrm{d}y, \tag{3.5a}$$

where τ is the along-front averaged horizontal slope-water Reynolds stress

$$\tau = -\langle u_1 v_1\rangle, \tag{3.5b}$$

where

$$\langle(*)\rangle = \lambda^{-1}\int_0^{\lambda}(*)\,\mathrm{d}x. \tag{3.5c}$$

The first term on the right-hand side of (3.5*a*) is responsible for any barotropic instability that might occur in the surrounding shelf-water current. The second term governs the baroclinic energy transfer. It follows that *if baroclinic instability occurs, then on average the correlation between the perturbation cross-shelf flow in the slope water and the frontal height anomaly must be positive.* Physically, we can interpret positive (negative) h as a cold (warm) anomaly in the slope water. Hence a positive correlation between v_1 and h can be interpreted as net onshore transport of heat. The onshore heat flux can be viewed as resulting from the fact that the instability occurs owing to the offshore 'slumping' of the coupled density front and the concomitant release of potential energy due to the stratification.

If (3.3*b*) is multiplied by h, then we can form the balance

$$\frac{\partial}{\partial t}\int_{a_1}^{a_2}(\mu h_{0_y})^{-1}\langle h^2\rangle\,\mathrm{d}y = -2\int_{a_1}^{a_2}\langle v_1 h\rangle\,\mathrm{d}y. \tag{3.6}$$

This expression and (3.5*a*) can be combined to form

$$\frac{\partial}{\partial t}\left[\int_{-B}^{\infty}\langle\nabla\eta\cdot\nabla\eta\rangle\,\mathrm{d}y + \int_{a_1}^{a_2}(\mu h_{0_y})^{-1}\langle h^2\rangle\,\mathrm{d}y\right] = 2\int_{-B}^{\infty}\tau U_{0_y}\,\mathrm{d}y. \tag{3.7}$$

Hence in the 'pure' baroclinic problem (i.e. $U_{0_y} = 0$), it immediately follows that *instability can only occur if* $h_{0_y}(y) < 0$ *for some values of* $y \in (a_1, a_2)$. *Conversely, it follows*

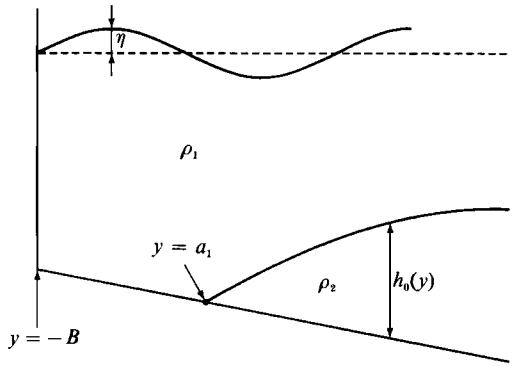

FIGURE 2. An example of an isolated density front on a sloping continental shelf which would be baroclinically stable according to our theory. The front height satisfies $h_{0_y} > 0$ but $h_{0_{yy}} < 0$ so that $h_0(y) \to$ constant as $y \to \infty$.

that if $h_{0_y}(y) > 0$ *for all* $y \in (a_1, a_2)$, *then the front is linearly stable in the sense of Liapounov.* In figure 2 we give a sketch of a semi-infinite stable front on a sloping continental shelf (for which $h_{0_y}(y) > 0$ and $h_0(y)$ remains finite).

These results can be easily interpreted in the context of the potential vorticity associated with the coupled density front. The potential vorticity associated with the front equations (2.9*a*, *b*) is given by $\text{PV} = [s\hat{\boldsymbol{e}}_3 \cdot (\boldsymbol{\nabla} \times \boldsymbol{u}_2) + 1]/h$. In the limit $s \to 0$ we have $\text{PV} \approx 1/h_0 + O(s)$. Therefore the above necessary condition for baroclinic instability is equivalent to requiring $\text{PV}_y \approx -h_{0_y}/h_0^2 > 0$ for some values of $y \in (a_1, a_2)$, i.e. the leading-order (in s) frontal potential vorticity must contain regions where it is increasing in the *offshore* direction for baroclinic instability to occur. Conversely, if the leading-order frontal potential vorticity were to increase in the *onshore* direction for all $y \in (a_1, a_2)$, then the front would be linearly stable.

3.3. *The along-front normal-mode equations*

In the remainder of this paper we focus on along-front-propagating normal-mode instabilities of the form

$$[\eta, h, \phi_1, \phi_2] = [\tilde{\eta}(y), \tilde{h}(y), \tilde{\phi}_1, \tilde{\phi}_2] \exp[\mathrm{i}k(x - ct)] + \text{c.c.}, \tag{3.8}$$

where c.c. means complex conjugate, k is the along-shelf wavenumber and c is the along-front complex phase speed. Substitution of (3.8) into (3.3) and (3.4) yields (after dropping the tildes and eliminating $\tilde{h}(y)$ in (3.3*a*) using (3.3*b*))

$$(c - \mu U_0)(\eta_{yy} - k^2\eta) + [1 + \mu U_{0_{yy}} + \mu h_{0_y}(c - 1 - \mu U_0)^{-1}]\eta = 0, \tag{3.9a}$$

$$h = \mu h_{0_y}(c - 1 - \mu U_0)^{-1}\eta, \tag{3.9b}$$

in the frontal region $a_1 < y < a_2$. In the non-frontal regions $-B < y < a_1$ and $y > a_2$, the problem for $\eta(y)$ is given by

$$(c - \mu U_0)(\eta_{yy} - k^2\eta) + (1 + \mu U_{0_{yy}})\eta = 0. \tag{3.10}$$

Equation (3.10) is simply a Rayleigh stability equation which includes the effect of the vorticity gradient associated with the topographic beta-plane. Note that there is a sign change in the 'beta' effect (i.e. the coefficient of the 'one' in the last term in (3.10)) compared to the usual way the Rayleigh stability equation is written on a planetary beta-lane (LeBlond & Mysak 1978, §44) because of the orientation of our horizontal coordinates (see figure 1). Equation (3.9*a*), which governs $\eta(y)$ over the

frontal region $a_1 < y < a_2$, is of the same form as (3.10) except that (3.9*a*) also contains the additional term $\mu h_{0_y}(c-1-\mu U_0)^{-1}$ which, as we shall see, drives the baroclinic instability.

The boundary conditions at $y = a_1$ and a_2 for the normal modes can be written in the form

$$\left.\begin{aligned} h + h_{0_y}\phi_{1,2} &= 0 \\ (c-1-\mu U_0)\phi_{1,2} &= -\mu\eta \end{aligned}\right\} \quad \text{on} \quad y = a_{1,2}, \tag{3.11a, b}$$

respectively, where we have eliminated the $h(a_{1,2})$ term in (3.4*c*, *d*) using (3.4*a*, *b*). The boundary condition (3.4*e*) becomes simply

$$\eta = 0 \quad \text{on} \quad y = -B, \tag{3.12}$$

and (3.4*f*) remains unchanged. It turns out that for the normal-mode solutions the boundary conditions (3.11*a*, *b*) and the frontal continuity equation (3.9*b*) are not independent. If (3.9*b*) is evaluated at $y = a_1$ or a_2 and substituted into (3.11*a*), the resulting expression can be rearranged into exactly (3.11*b*) assuming $h_{0_y}(a_{1,2}) \neq 0$. This dependence implies that the mathematical problem of solving (3.9*a*, *b*) together with (3.11*a*, *b*) is not enough to fully specify the solution.

The resolution to this apparent difficulty is to require that the pressure and normal mass flux in the slope water be continuous across the frontal boundaries $y = a_{1,2}$. For our problem formulation these matching conditions can be written in the form

$$\left.\begin{aligned} [(c-U_0)\eta_y + U_{0_y}\eta] &= 0 \\ [(U_0-c)^{-1}\eta] &= 0 \end{aligned}\right\} \text{ on } \quad y = a_{1,2}, \tag{3.13a, b}$$

respectively, for the continuity of pressure and normal mass flux across the frontal edges (LeBlond & Mysak 1978, §45). In (3.13*a*, *b*), $[(*)] = (*)(a_{1,2}^+) - (*)(a_{1,2}^-)$, i.e. the jump in (*) across $y = a_{1,2}$. The matching conditions (3.13*a*, *b*) also apply across any point where $U_0(y)$ or $U_0'(y)$ is discontinuous.

We have been able to solve the above equations exactly for a simple parabolic coupled density front configuration. This solution will be presented in §4. In our subsequent analysis we shall focus directly on the 'pure' baroclinic problem in which $U_0 = 0$.

3.4. *General stability results for the normal modes*

In this subsection we present several qualitative results for the normal-mode equations including: necessary instability conditions, phase speed bounds, a semicircle theorem, demonstrate the existence of a high along-front wavenumber cutoff and the necessity of a minimum interaction parameter for instability. It turns out that because the complex phase speed occurs quadratically in the stability equation (3.9*a*) the usual derivations of the above instability conditions are not useful here because the results that would be obtained are complicated expressions involving mean flow variables and undetermined perturbation quantities which are difficult to interpret. In addition, the usual derivations of the semicircle theorems on a beta-plane require a *Poincaré inequality* which because of our semi-infinite domain will not exist.

Multiplying (3.9*a*) and (3.10) by the complex conjugate of $\eta(y)$, integrating the result over y, and adding the two equations together gives the balance

$$\int_{-B}^{\infty} \left\{ \left[(1-ck^2) + \frac{(c^*-1)}{|c-1|^2}\mu h_{0_y}\Theta(y) \right] |\eta|^2 - c|\eta_y|^2 \right\} dy = 0, \tag{3.14}$$

where $\Theta(y) = 1$ for $a_1 < y < a_2$, and $\Theta(y) = 0$ for $-B < y \leqslant a_1$ and $a_2 \leqslant y < \infty$, and c^* is the complex conjugate of $c = c_R + ic_I$. The imaginary and real parts of (3.14) are given by, respectively,

$$c_I \left\{ \int_{-B}^{\infty} [|\eta_y|^2 + (k^2 + \mu h_{0_y} \Theta / |c-1|^2)|\eta|^2] \, dy \right\} = 0, \tag{3.15}$$

$$c_R \left\{ \int_{-B}^{\infty} [|\eta_y|^2 + (k^2 - \mu h_{0_y} \Theta / |c-1|^2)|\eta|^2] \, dy \right\} = \int_{-B}^{\infty} [1 - \mu h_{0_y} \Theta / |c-1|^2] \, |\eta|^2 \, dy. \tag{3.16}$$

From (3.15) we have two immediate results. *If $\mu = 0$ then the integrand is strictly positive for non-trivial solutions implying $c_I = 0$ and therefore the front is neutrally stable.* This shows the necessity of the baroclinicity for instability. Note that it also follows from (3.15) that *a necessary condition for instability is that $h_{0_y}(y) < 0$ for some values of $a_1 < y < a_2$.* (We have already shown that this result follows from (3.7).) Consequently, assuming that instability occurs we may set

$$\min_{y \in (a_1, a_2)} h_{0_y}(y) = -\gamma^2 < 0 \quad (\gamma > 0), \tag{3.17}$$

which will be used below.

Assuming that instability occurs ($c_I \neq 0$ implies instability since it is easy to see from (3.9) that the phase speed c always comes in complex-conjugate pairs if c is complex), the expression inside the curly brackets in (3.15) must be identically zero and can be rearranged into the form

$$|c-1|^2 = -\mu Q^{-1} \int_{-B}^{\infty} \Theta h_{0_y} |\eta|^2 \, dy, \tag{3.18}$$

where

$$Q = \int_{-B}^{\infty} (|\eta_y|^2 + k^2 |\eta|^2) \, dy > 0. \tag{3.19}$$

However, using (3.17) it follows from (3.18) that

$$\begin{aligned} |c-1|^2 &\leqslant \mu \gamma^2 Q^{-1} \int_{-B}^{\infty} \Theta |\eta|^2 \, dy, \\ &\leqslant \mu \gamma^2 Q^{-1} \int_{-B}^{\infty} |\eta|^2 \, dy, \\ &= (\mu \gamma^2 / k^2) Q^{-1} \int_{-B}^{\infty} k^2 |\eta|^2 \, dy, \\ &\leqslant (\mu \gamma^2 / k^2). \end{aligned} \tag{3.20}$$

From (3.20) it follows that *if instability occurs, then the complex phase speed must lie in the semicircle defined by*

$$(c_R - 1)^2 + c_I^2 \leqslant \mu \gamma^2 / k^2, \tag{3.21a}$$

where γ^2 is determined from (3.17). Note that the radius of the semicircle will increase with increasing μ but will decrease with increasing along-front wavenumber k. As well, it follows from (3.21a) that the growth rate satisfies

$$\sigma = k c_I \leqslant \gamma \mu^{\frac{1}{2}}. \tag{3.21b}$$

We can get alternate bounds on the real part of the phase speed as follows. Assuming instability occurs we may eliminate $|c-1|^2$ in the integrands in (3.16) using (3.18). The result can be written in the form

$$c_R = \tfrac{1}{2} + (2Q)^{-1} \int_{-B}^{\infty} |\eta|^2 \, dy. \tag{3.22}$$

It follows immediately from (3.22) that *if instability occurs the real phase speed must lie in the interval*

$$0.5 \leqslant c_R \leqslant 0.5 + (2k^2)^{-1}, \tag{3.23}$$

where the right-hand inequality is obtained similarly to (3.20). *Conversely, if* c_R *lies outside the interval* (3.23) *the mode must be neutrally stable.*

The existence of a high-wavenumber cutoff can be inferred directly from (3.21*a*) and (3.23). It follows from (3.21*a*) that the real part of the complex phase speed of an unstable mode must lie in the interval

$$1 - \mu^{\frac{1}{2}}\gamma/k \leqslant c_R \leqslant 1 + \mu^{\frac{1}{2}}\gamma/k. \tag{3.24}$$

Clearly, for sufficiently large along-front wavenumbers (for a given $\mu^{\frac{1}{2}}\gamma$) the intervals (3.23) and (3.24) will be disjoint since the interval in (3.23) collapses to a small neighbourhood immediately above $c_R = 0.5$ and (3.24) collapses to a small neighbourhood centred at $c_R = 1.0$. Consequently, it follows that *instability can only occur when*

$$0.5 + (2k^2)^{-1} \geqslant 1 - \mu^{\frac{1}{2}}\gamma/k, \tag{3.25a}$$

which is the necessary and sufficient condition for the intersection of the two intervals (3.23) and (3.24) to be non-empty. The inequality (3.25*a*) can be rearranged to yield

$$0 \leqslant k \leqslant k_{\max} = \mu^{\frac{1}{2}}\gamma + [1 + \mu\gamma^2]^{\frac{1}{2}}, \tag{3.25b}$$

where we have restricted attention, without loss of generality, to non-negative wavenumbers. *Consequently, unstable normal modes necessarily have along-front wavenumbers which satisfy* (3.25*b*) *and, conversely, normal modes with the property* $k \geqslant k_{\max}$ *are necessarily neutrally stable.* The wavenumber $k_{\max}$ will be an overestimate of the high-wavenumber cutoff as a function of γ and μ.

The inequality (3.25*b*) can be rearranged to show that, depending on the wavenumber, a minimum $\gamma\mu^{\frac{1}{2}}$ is required for instability. Note that $k_{\max} \geqslant 1$ for all γ and μ. Thus wavenumbers in the range $0 \leqslant k \leqslant 1$ will always satisfy (3.25*b*) but wavenumbers for which $k \geqslant 1$ may not satisfy (3.25*b*) depending on the magnitudes of μ and γ. It follows from (3.25*a*) that *a necessary condition for a normal mode with along-front wavenumber k to be unstable is that*

$$\gamma\mu^{\frac{1}{2}} \geqslant (k^2 - 1)/(2k). \tag{3.26}$$

Clearly, if $0 \leqslant k \leqslant 1.0$, then (3.26) is satisfied for all (positive) γ and μ. But if $k \geqslant 1$ a minimum $\gamma\mu^{\frac{1}{2}}$ is required for instability.

4. An exact solution for a parabolic coupled front

In this section we present the exact solution that can be obtained for a parabolic coupled density front of the form

$$h_0(y) = 1 - (y/a)^2. \tag{4.1}$$

The unperturbed lateral frontal boundaries in (2.16) are given by $a_2 = -a_1 = a$.

For the parabolic front (4.1), it follows from (3.18) that $\gamma^2 = 2/a$ and thus the semicircle of instability will be given by

$$(c_R - 1)^2 + c_I^2 \leqslant 2\mu(ak^2)^{-1}. \tag{4.2}$$

The high-wavenumber cutoff (3.25b) will be given by

$$k_{max} = (2\mu/a)^{\frac{1}{2}} + [1 + 2\mu/a]^{\frac{1}{2}}. \tag{4.3a}$$

Thus broader coupled fronts will have a reduced interval of unstable wavenumbers than narrower fronts. Given a particular wavenumber, the estimated minimum interaction parameter needed for instability as determined by (3.26) is given by

$$\mu_{min} = a(k^2 - 1)^2/(8k^2), \tag{4.3b}$$

if $k > 1$, and $\mu_{min} = 0$ for $0 \leqslant k \leqslant 1$. The value of μ_{min} in (4.3b) would be an underestimate.

4.1. *Derivation of the dispersion relation*

Substitution of $U_0 = 0$ and $h_0(y)$ given by (4.1) into the normal-mode equations (3.9a) and (3.10) yields the problem

$$\eta_{yy} - \{k^2 - c^{-1} + 2\mu[a^2 c(c-1)]^{-1} y\}\eta \quad \text{for} \quad |y| < a, \tag{4.4a}$$

$$\eta_{yy} - \{k^2 - c^{-1}\}\eta = 0 \quad \text{for} \quad -B < y - a \quad \text{and} \quad y > a, \tag{4.4b}$$

with the boundary conditions

$$\eta = 0 \quad \text{on} \quad y = -B, \tag{4.5a}$$

$$\eta \to 0 \quad \text{as} \quad y \to +\infty, \tag{4.5b}$$

and the pressure and mass flux matching conditions

$$[\eta] = [\eta_y] = 0 \quad \text{on} \quad y = \pm a. \tag{4.6}$$

The general solution to (4.4a) may be written in the form

$$\eta(y) = \alpha_1 \operatorname{Ai}[\xi(y)] + \alpha_2 \operatorname{Bi}[\xi(y)] \quad \text{for} \quad |y| < a, \tag{4.7a}$$

where $\operatorname{Ai}(\xi)$ and $\operatorname{Bi}(\xi)$ are Airy functions (Abramowitz & Stegun 1972, §10.4) with argument $\xi(y)$ given by

$$\xi(y) = [ca^2(c-1)(2\mu)^{-1}]^{\frac{2}{3}}\{k^2 - c^{-1} + 2\mu y[c(c-1)a^2]^{-1}\}, \tag{4.7b}$$

and where α_1 and α_2 are, as yet, undetermined coefficients. The solutions to (4.4b) and (4.5a, b) may be written in the form, respectively,

$$\eta(y) = \alpha_3 \sinh[(k^2 - c^{-1})^{\frac{1}{2}}(y + B)] \quad \text{for} \quad -B < y < -a, \tag{4.8}$$

$$\eta(y) = \alpha_4 \exp[-(k^2 - c^{-1})^{\frac{1}{2}} y] \quad \text{for} \quad y > a, \tag{4.9}$$

where α_3 and α_4 are additional, as yet, undetermined coefficients. We take our branch cut in the complex plane along the negative real axis.

The application of the matching conditions (4.6) is straightforward and leads to a system of four homogeneous equations in the unknown coefficients $\alpha_1, \alpha_2, \alpha_3$ and α_4. This system can be most conveniently written in the matrix form

$$\boldsymbol{M} \cdot \boldsymbol{\alpha} = \boldsymbol{0}, \tag{4.10}$$

where $\boldsymbol{\alpha} = (\alpha_1, \alpha_2, \alpha_3, \alpha_4)^{\mathrm{T}}$ (i.e. a column vector) and $\boldsymbol{M} = [M_{ij}]$ is the 4×4 matrix with components given by

$$\left.\begin{aligned}
&M_{11} = \mathrm{Ai}(\xi^-), \quad M_{12} = \mathrm{Bi}(\xi^-),\\
&M_{13} = -\sinh[(k^2 - c^{-1})^{\frac{1}{2}}(B-a)], \quad M_{21} = \mathrm{Ai}_\xi(\xi^-),\\
&M_{21} = \mathrm{Bi}_\xi(\xi^-), \quad M_{31} = \mathrm{Ai}(\xi^+), \quad M_{32} = \mathrm{Bi}(\xi^+),\\
&M_{23} = -[c(c-1)\,a^2(2\mu)^{-1}]^{\frac{1}{3}}(k^2 - c^{-1})^{\frac{1}{2}}\cosh[(k^2 - c^{-1})^{\frac{1}{2}}(B-a)],\\
&M_{33} = -\exp[-(k^2 - c^{-1})^{\frac{1}{2}}a], \quad M_{41} = \mathrm{Ai}_\xi(\xi^+), \quad M_{42} = \mathrm{Bi}_\xi(\xi^+),\\
&M_{14} = M_{24} = M_{33} = M_{34} = 0,
\end{aligned}\right\} \tag{4.11}$$

where $\xi^+ = \xi(+a)$ and $\xi^- = \xi(-a)$. For a non-trivial solution of (4.10) we require

$$\det(\boldsymbol{M}) = 0, \tag{4.12a}$$

which forms the complex dispersion relationship for the normal-mode solutions. We may consider that (4.12a) implicitly defines a four-parameter dispersion relationship of the form

$$c = \hat{c}(k, \mu, a, B). \tag{4.12b}$$

4.2. *Description of the solutions to the dispersion relationship*

In this subsection we give a qualitative description of the solutions to the dispersion relation (4.12). As it turns out, the most important parameters that influence the stability characteristics are the along-front wavenumber k and the baroclinic interaction parameter μ. This is not to say that variations in the width of the front (i.e. $2a$) or the distance the front is from the shore (i.e. $|B-a|$) are unimportant, but rather the role that these parameters play is largely secondary to the role played by variations in the other two parameters. In particular, we found that once the shore distance $|B-a|$ was even slightly larger than zero, the growth rate, frequency and spatial characteristics of the modes varied very little as B was further increased. This can be very easily interpreted. On the onshore side of the front, the frontal height satisfies $h_{0_y}(y) > 0$. However, this means that the onshore side of the front does not, locally, satisfy the necessary condition for instability (3.17). Consequently, we may expect that on the onshore side the frontal boundary perturbation will not be very pronounced (see figure 9a) and the location of the shore will not play a significant role in the stability characteristics. For the calculations described here, we set $B = 2a$ so that the front is a dimensional distance of aL (L is the internal deformation radius) from the shore. Our choice for B will be advantageous for the contour plots of the various flow fields to be shown.

The principal effect of varying the width of the front can be easily seen using (4.2) and (4.3). Roughly speaking, increasing (decreasing) the front width parameter a, keeping the other parameters fixed, will lead to decreased (increased) growth rates and along-front phase speeds which are contained in a narrower (broader) band about 1.0, a decreased (increased) high-wavenumber cutoff, and an increased (decreased) minimum interaction parameter that is needed for instability. Thus the stability boundary shown in figure 3 would be shifted up (down) for decreased (increased) a. For the purposes of our discussion here we take $a = 1.0$ which corresponds to the dimensional width of the unperturbed front being twice the internal deformation radius. (Hence the shore will be a distance of one internal deformation radius away from the nearest unperturbed frontal boundary.) We feel that this value for the front width is not inconsistent with the oceanographic and laboratory observations described earlier.

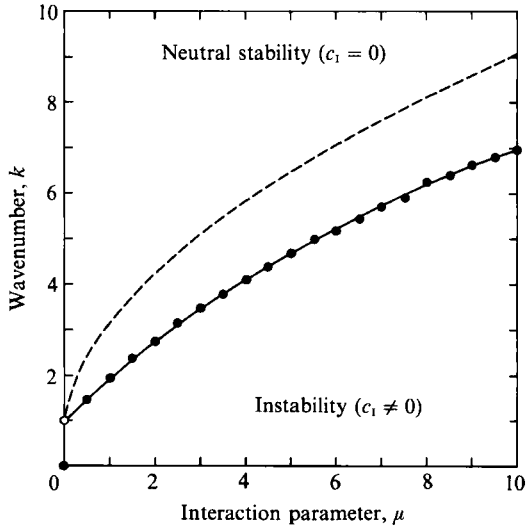

FIGURE 3. Stability diagram in the μ–k parameter plane for the quadratic front given by (4.1). The solid curve is the high-wavenumber cutoff as computed from the dispersion relation (4.12). The dashed line is the estimated high wavenumber cutoff given by (4.3a).

Figure 3 is a stability diagram in the μ–k parameter plane, with $a = 1.0$ and $B = 2.0$. The solid line is the high-wavenumber cutoff as computed directly from the dispersion relationship (4.12a). The dashed line is the estimated cutoff given by (4.3a). Our calculations indicated that the limit $\mu \to 0^+$ of the computed high-wavenumber cutoff as determined by the dispersion relation is singular in the following sense. As we took $\mu \to 0^+$, the limit of the cutoff appeared to be one (which is what (4.3a) suggests). However, in accordance with (3.21b), the computed growth rates for the unstable wavenumbers approached zero as μ became vanishingly small. Thus although in the limit as $\mu \to 0^+$ the computed cutoff appeared to approach one, the growth rates for the wavenumbers that are less than one all vanish. We have decided to depict this limiting behaviour by placing an open circle at $k = 1.0$ and placing a dot at $k = 0$ for $\mu = 0$ indicating that even though the cutoff limit was formally one, all wavenumbers are in fact neutrally stable when $\mu = 0$.

Throughout this section it will be useful to convert the non-dimensional calculations back into dimensional form. The scalings presented in §2 imply a horizontal length scale of about $L \approx 15$ km, an advective timescale of about $T \approx 7$ days, and a velocity scale of about $U_* \approx 2.5$ cm/s. Consequently, if we let σ be the non-dimensional growth rate (i.e. $\sigma = kc_I$ where c_I is the imaginary part of the complex phase speed c and k is the along-front wavenumber), then the corresponding dimensional e-folding time for an unstable mode, denoted T_E^*, is given by $T_E^* \approx (7\sigma^{-1})$ days. The dimensional frequency of a normal mode, denoted ω^*, and the dimensional period, denoted P^*, are related to the non-dimensional frequency, denoted ω (i.e. $\omega = kc_R$ where c_R is the real part of the complex phase speed c), through the relations $\omega^* \approx (\omega/7)(\text{days})^{-1}$ and $P^* = 2\pi/\omega^* \approx (44/\omega)$ days, respectively. The dimensional along-front wavelength, denoted λ^*, of a normal mode is related to the non-dimensional wavenumber through the relation $\lambda^* = 2\pi L/k \approx (94/k)$ km. The dimensional along-front phase velocity, denoted c^*, is given by $c^* = 2.5c_R$ cm/s.

In figures 4, 5 and 6 we present the non-dimensional growth rates, frequencies and along-front phase speeds obtained from the dispersion relation for values of μ of 0.1,

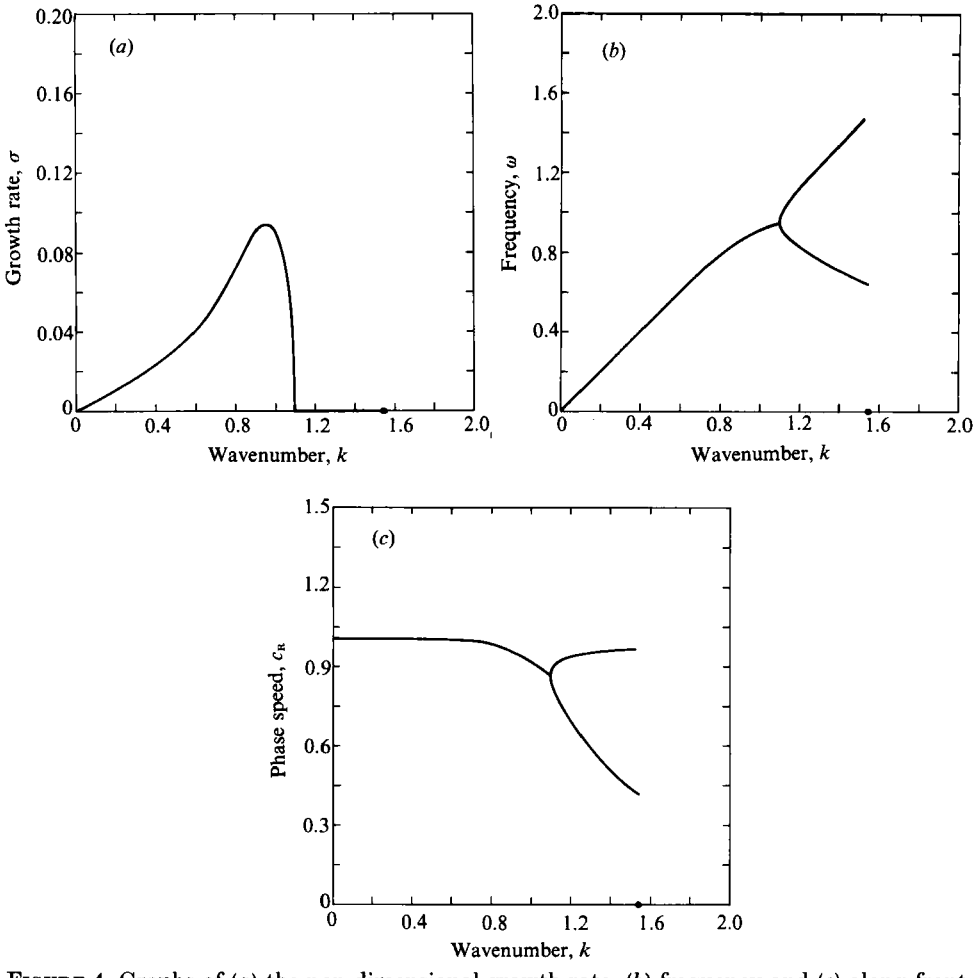

FIGURE 4. Graphs of (*a*) the non-dimensional growth rate, (*b*) frequency and (*c*) along-front phase speed versus the along-front wavenumber k for $\mu = 0.1$. The dot on the wavenumber axis is k_{max} as determined by (4.3*a*).

μ	0.1	2.0	5.0
k, λ^*	0.958, 98 km	1.421, 66.1 km	2.15, 43.7 km 1.18, 79.6 km
ω, P^*	0.858, 51.3 days	1.336, 32.9 days	2.657, 16.6 days 0.795, 55.3 days
σ, T_E^*	0.094, 74.4 days	0.849, 8.2 days	1.573, 4.4 days 0.228, 30.8 days
c_R, c^*	0.896, 2.2 cm/s	0.939, 2.3 cm/s	1.236, 3.1 cm/s 0.674, 1.7 cm/s

TABLE 1. Non-dimensional and dimensional stability characteristics for the most unstable modes for $\mu = 0.1$, 2.0 and 5.0, respectively. For $\mu = 5.0$ we have included two entries: the top and bottom lines correspond to the most unstable mode on the upper and lower growth rate curves, respectively, shown in figure 6(*a*).

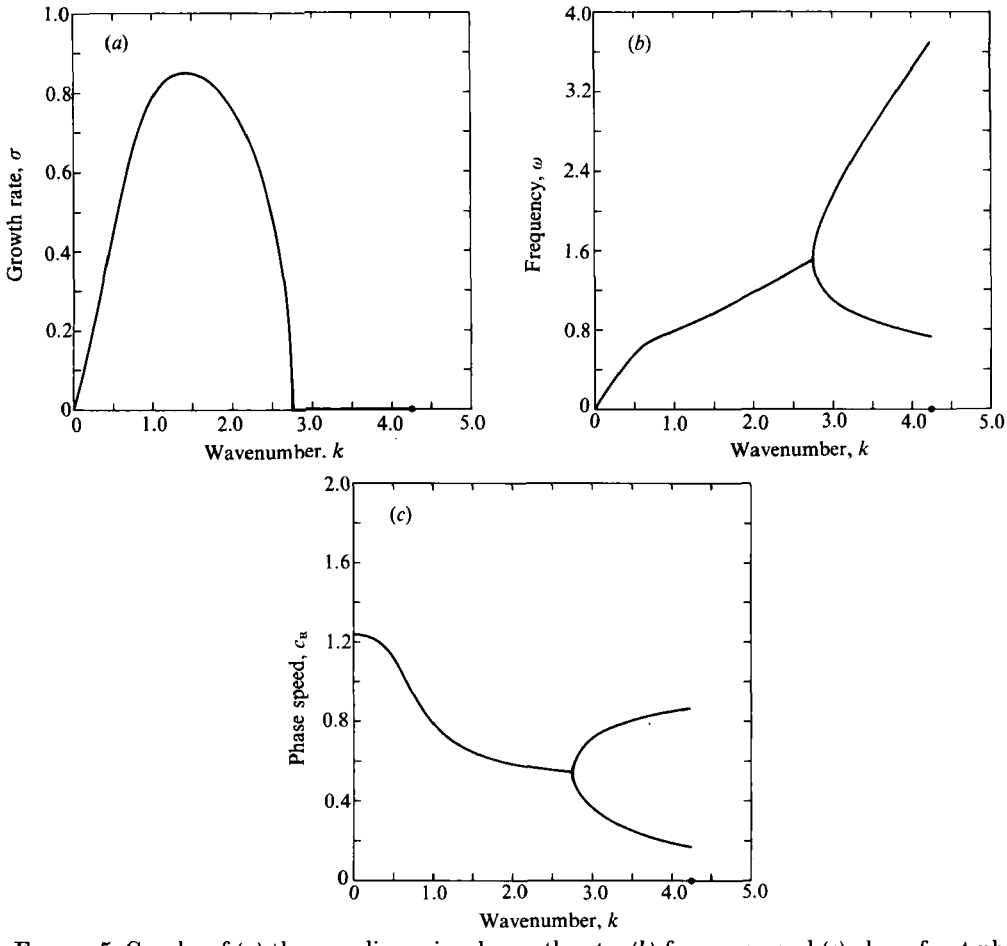

FIGURE 5. Graphs of (*a*) the non-dimensional growth rate, (*b*) frequency and (*c*) along-front phase speed versus the along-front wavenumber k for $\mu = 2.0$. The dot on the wavenumber axis is $k_{\max}$ as determined by (4.3*a*).

2.0 and 5.0, respectively, as a function of the along-front wavenumber for the interval $0 \leqslant k \leqslant k_{\max}$ where $k_{\max}$ is determined from (3.25*b*). The location of $k_{\max}$ is depicted on the horizontal axes of figures 4, 5 and 6. These interaction parameter values will correspond to 'small', 'typical' and 'large' values of μ, respectively, as suggested by our parameter estimates in §2. The stability characteristics for the most unstable modes for $\mu = 0.1$, 2.0 and 5.0 are given in table 1.

The $\mu = 0.1$ solutions show relatively long, low-frequency slowly growing modes because of the relatively inefficient transfer of mean potential energy to perturbation kinetic energy that a small value of μ implies (or, equivalently, the strong influence of the stabilizing topographic beta-plane). Another aspect to note for these low-μ solutions is that over a range of unstable wavenumbers near $k \approx 0$ these modes are relatively non-dispersive as can be seen by examining figures 4(*b*) and 4(*c*). The mathematical reason for this follows easily enough from the basic model (2.10). If μ is small enough, (2.10*b*) is approximately a non-dispersive unidirectional wave equation with propagation velocity $+1.0$.

Figure 5 depicts the growth rates, frequencies and phase speeds that occur for $\mu = 2.0$ as a function of the wavenumber. This value of the interaction parameter is

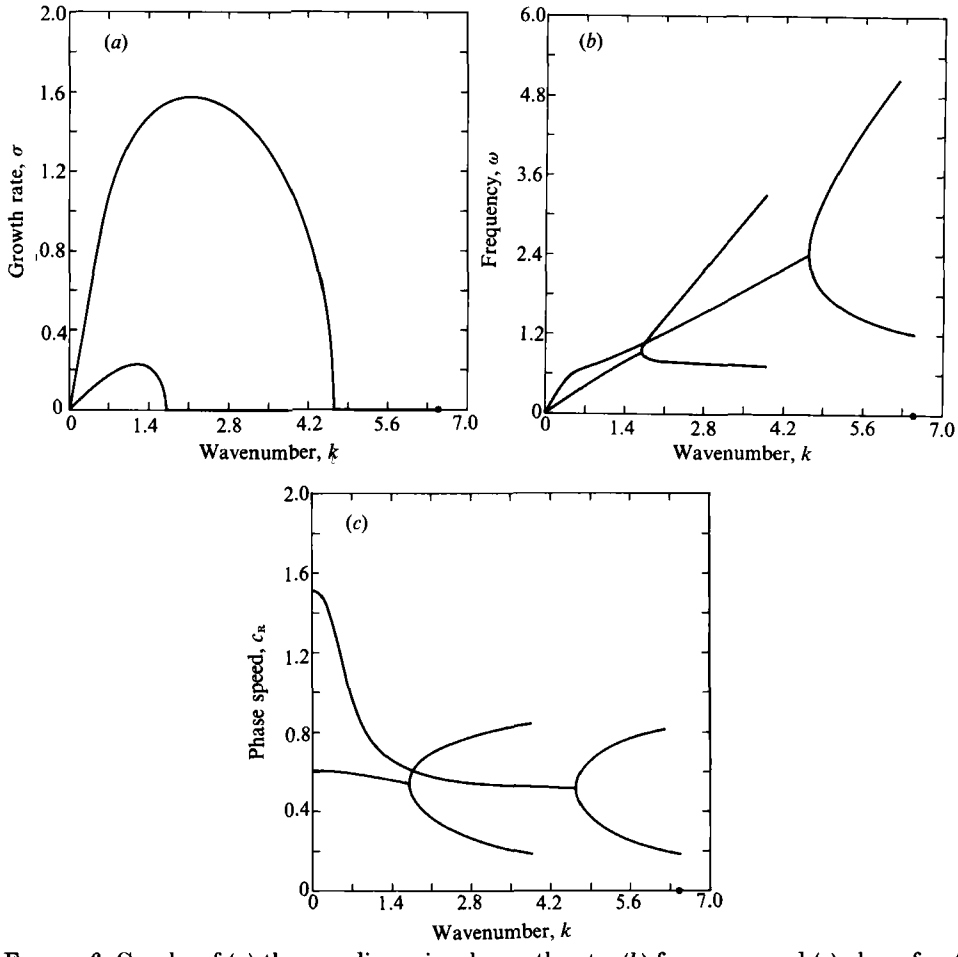

FIGURE 6. Graphs of (*a*) the non-dimensional growth rate, (*b*) frequency and (*c*) along-front phase speed versus the along-front wavenumber k for $\mu = 5.0$. The dot on the wavenumber axis is $k_{\max}$ as determined by (4.3*a*).

approximately the value suggested by the scalings adopted in §2. For this value of μ, our solutions show only a single unstable branch. However these modes, unlike those shown in figure 4, are strongly dispersive. In general, the range of unstable wavenumbers has increased as have the growth rates at each wavenumber.

The solutions for $\mu = 5.0$ shown in figure 6 are qualitatively different than the solution for $\mu = 0.1$ and 2.0 in that for this value of the interaction parameter a second unstable branch has formed. The curve with the smaller growth rates corresponds to the branches shown in figures 4 and 5. The curve with the smaller growth rates is a new unstable branch of solutions that does not exist for $\mu \lesssim 3.48$ (see figure 7). We shall show in §4.3 that the instabilities on the branch with the larger growth rates have horizontal configurations which are monopole-like in appearance (see figure 9), whereas the instabilities on the branch with the smaller growth rates have horizontal configurations which are dipole-like in appearance (see figure 10).

The development of the second branch of unstable solutions is shown in figure 7 where we plot the growth rate of wavenumber $k = 1.18$ versus the interaction

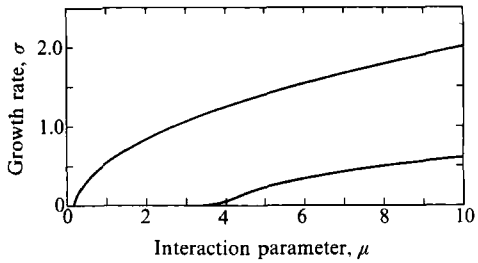

FIGURE 7. Graph of the computed growth rates versus the interaction parameter μ for an along-front wavenumber $k = 1.18$. This wavenumber corresponds to the most unstable mode for the smaller-growth-rate branch of instabilities depicted in figure 6(*a*).

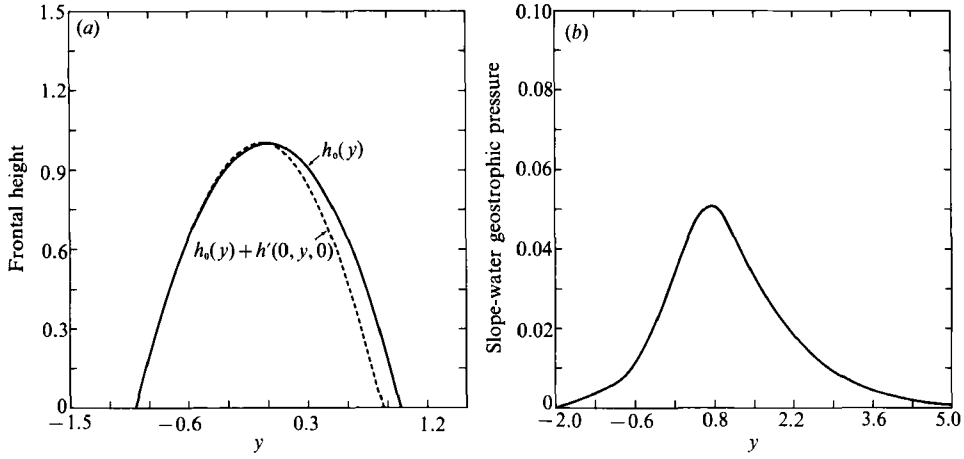

FIGURE 8. (*a*) A cross-shelf section of the unperturbed frontal height $h_0(y) = 1-(y/a)^2$ and the total frontal height $h_0(y)+h'(x=0,y,t=0)$ for the most unstable $\mu = 2.0$ mode. Note that there is very little perturbation on the shoreward side of the front. (*b*) A cross-shelf section of the perturbation geostrophic pressure $\eta'(x=0,y,t=0)$ in the slope water for the most unstable $\mu = 2.0$ mode.

parameter μ over the range $0 \leqslant \mu \leqslant 10$. This wavenumber was chosen because it is the non-dimensional wavenumber of the most unstable mode on the lower-growth-rate curve in figure 6(*a*). Note that there is an interval (i.e. $0 \leqslant \mu \lesssim 0.13$) for which this wavenumber will correspond to a neutrally stable mode. The estimate provided by (4.3) for the minimum μ needed for the instability of a mode with wavenumber $k = 1.18$ would be $\mu_{\min} \approx 0.014$. The second unstable branch in figure 7 begins to develop when $\mu \approx 3.48$. As μ continues to increase, the growth rate of both modes monotonically increases. We have been unable to find the generation of a third unstable branch for the range of μ that we examined.

4.3. *Spatial structure of the unstable modes*

In this subsection we describe the spatial structure of the most unstable mode for the interaction parameter $\mu = 2.0$ (which is a 'typical' oceanographic estimate for μ). As well, we shall briefly describe the spatial structure of the most unstable solution on the smaller-growth-rate branch of instabilities for $\mu = 5.0$ (see figure 6*a*). We choose the perturbation frontal height to be about 10% of the unperturbed height.

In figure 8(*a*) we show a cross-shelf section taken from the unperturbed frontal height and total frontal height $h_0(y)+h'(x=0,y,t=0)$. The region where the

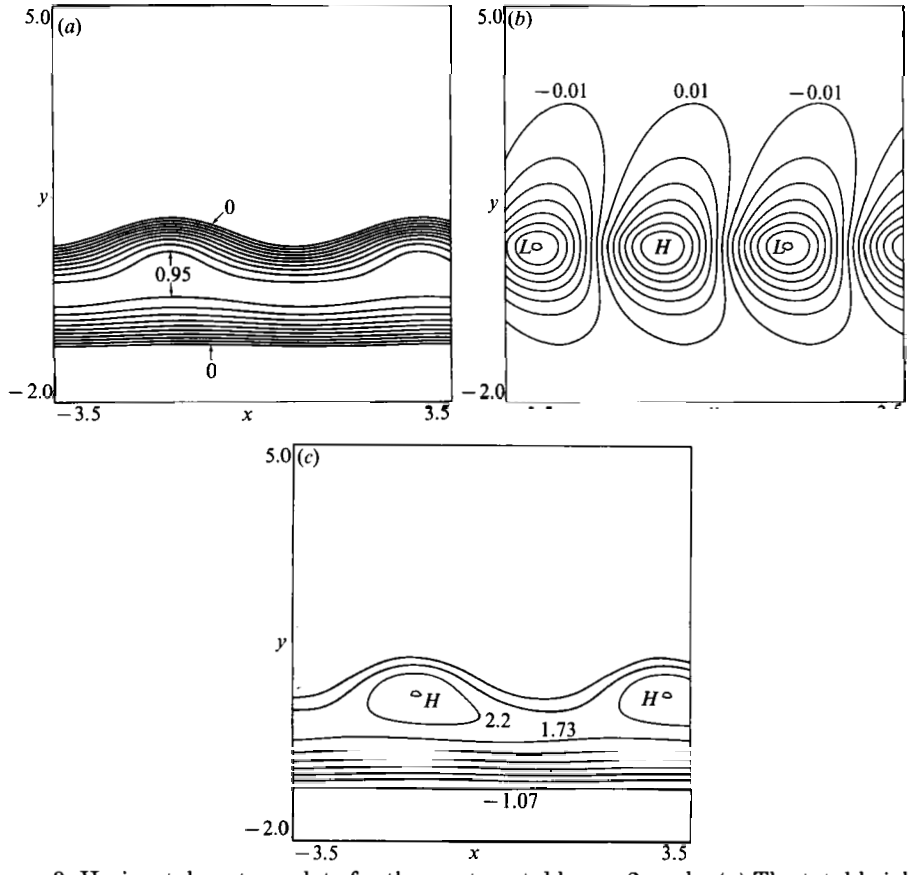

FIGURE 9. Horizontal contour plots for the most unstable $\mu = 2$ mode. (*a*) The total height of the perturbed coupled density front. The contour interval is $+0.105$. The perturbed lateral frontal boundaries are the zero height contour. (*b*) The geostrophic pressure field in the slope water associated with the destabilized front described in (*a*). The contour increments are ± 0.01 and the spatial scale is the same as in (*a*). (*c*) The total geostrophic pressure in the coupled density front as determined by (2.14*c*) associated with the destabilized front described in (*a*). The instability appears as a series of growing, propagating anticyclones on the off-shore side of the coupled density front. The contour intervals are ± 0.47.

perturbation anomaly is the largest is on the offshore section of the front where $h_{0_y}(y) < 0$. We interpret this as the result of the fact that on the onshore side of the front $h_{0_y}(y) > 0$ so that locally the necessary conditions for the instability are not met. On the offshore side, however, the front is free to 'shift' down the continental shelf and release potential energy (see also figure 9*a*). In figure 8(*b*) the corresponding transverse section for the slope-water geostrophic pressure is shown. There is a single cross-shelf extremum in the slope-water geostrophic pressure which occurs slightly offshore from the extremum in the perturbed frontal height.

In figure 9(*a–c*) we present horizontal contour plots of the total coupled front height, slope-water geostrophic pressure and total frontal pressure fields for the most unstable $\mu = 2.0$ mode. We can clearly see in figure 9(*a*) how the instability is intensified on the offshore side of the coupled front. Note that the lateral perturbations of the intersection of the front with the bottom are larger on the offshore side than on the onshore side. In figure 9(*b*) the corresponding geostrophic pressure field in the slope water is shown. The anomalies take the form of coastally

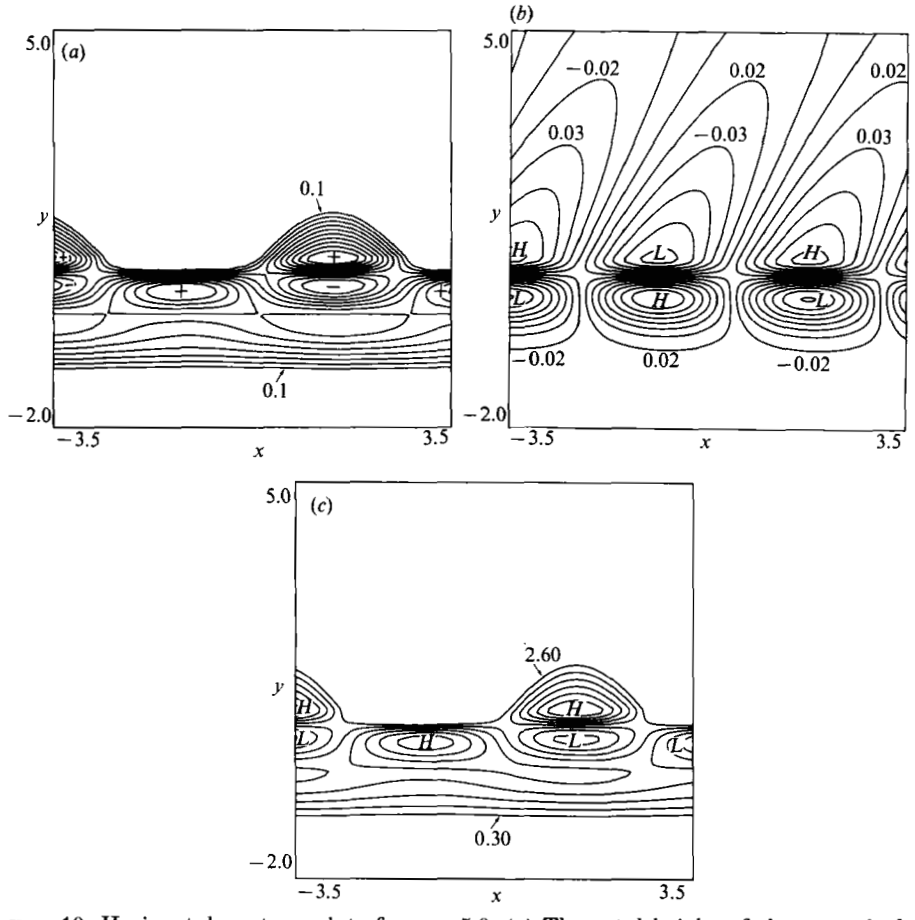

FIGURE 10. Horizontal contour plots for $\mu = 5.0$. (*a*) The total height of the perturbed coupled density for the most unstable mode on the lower-growth-rate branch of instabilities. The perturbed lateral frontal boundaries are the zero height contour. The contour interval is $+0.15$. (*b*) The geostrophic pressure field in the slope water associated with the destabilized front as described in (*a*). The contour interval is ± 0.01. (*c*) The total geostrophic pressure in the coupled density front as determined by (2.14*c*) associated with the destabilized front as described in (*a*). The contour interval is ± 1.15.

trapped topographic Rossby waves which, of course, have wavelengths and phase speeds as described above. In figure 9(*c*) we present the total geostrophic pressure field in the destabilized front. In figure 9(*b*, *c*) and 10(*b*, *c*) the H and L symbols denote regions of positive and negative pressure anomalies, respectively. The flow around the positive and negative pressure anomalies is, of course, anticyclonic and cyclonic, respectively.

In figure 10(*a*–*c*) we present horizontal contour plots of the total front height, slope-water geostrophic pressure and total frontal geostrophic pressure, respectively, for the most unstable mode on the smaller-growth-rate branch of instabilities for $\mu = 5.0$ (see figure 6*a*). These solutions are qualitatively different from the larger-growth-rate branch modes in that the perturbations take on a distinct dipole-like configuration in the offshore direction. In figure 10(*a*) the + and − signs denotes regions of positive and negative front height anomalies, respectively. Because of the relatively large value of μ in these solutions, the amplitude of the perturbation fields is larger than in the $\mu = 2.0$ solutions shown in figure 9.

5. Summary and conclusions

In this paper a theory has been developed to describe the baroclinic instability of a coupled density front on a linearly sloping continental shelf. The basic model we used corresponded to assuming that the surrounding slope water evolved quasi-geostrophically with the competing effects of the destabilizing baroclinic vortex-tube stretching/compression associated with the developing frontal anomalies and the stabilizing topographic vorticity gradient occurring simultaneously. However, the dynamics of the coupled density front while geostrophic was not, of course, quasi-geostrophic because deflections in the front thickness are not small in comparison with the scale height of the front itself. As a result, while the velocity fields in both the density front and slope water were geostrophically determined (but not uncoupled), the dynamical evolution of the height of the density front and the geostrophic pressure in the slope water were modelled as strongly interacting.

Several general stability properties were described. In particular, it was shown that the stability characteristics are determined in large part by an 'interaction' parameter denoted μ. If the along-front wavenumber of a normal-mode perturbation was larger than the inverse of the deformation radius, it was shown that a minimum non-zero μ was required for baroclinic instability. We were also able to show the existence of and obtain an estimate for a high-wavenumber cutoff, phase speed and growth-rate bounds. In addition, we obtained a new semicircle theorem for the unstable modes described in this paper.

For a parabolic coupled density front, the linear instability equations could be solved exactly and the spatial and temporal characteristics of the unstable modes described. For representative parameters (i.e. $\mu \approx 2.0$), the most unstable mode has a wavelength of about 66 km, an e-folding timescale of about 8 days, a period of about 33 days and a phase speed of about 2 cm/s. These instabilities take the form of growing topographic Rossby waves in the surrounding slope water. On the coupled front the instabilities take the form of amplifying anticyclones which are located on the offshore side of the front. This tendency was observed by GKS. It is tempting to suggest that as the instabilities continue to amplify, the anticyclones could separate from the coupled front and form cold-core isolated eddies such as described by Nof (1983) and Swaters & Flierl (1991). The theory developed in this paper therefore provides a mechanism for the generation of isolated cold-core eddies as a result of the baroclinic instability of coupled density fronts.

Preparation of this paper was supported in part by an Operating Research Grant awarded by the Natural Sciences and Engineering Research Council of Canada, and by a Science Subvention awarded by the Department of Fisheries and Oceans of Canada. We would also like to thank Mr Walter Aiello for programming assistance.

REFERENCES

ABRAMOWITZ, M. & STEGUN, J. A. 1972 *Handbook of Mathematical Functions*. Dover.

ARMI, L. & D'ASARO, E. 1980 Flow structures in the benthic ocean. *J. Geophys. Res.* **85**, 469–483.

CHARNEY, J. G. & FLIERL, G. R. 1981 Oceanic analogues of large-scale atmospheric motions. In *Evolution of Physical Oceanography – Scientific Surveys in Honor of Henry Stommel* (ed. B. A. Warren & C. Wunsch), pp. 504–548. The MIT Press.

COOPER, L. H. N. 1955 Deep water movements in the North Atlantic as a link between climatic changes around Iceland and biological productivity of the English Channel and Celtic Sea. *J. Mar. Res.* **14**, 347–362.

Cushman-Roisin, B. 1986 Frontal geostrophic dynamics. *J. Phys. Oceanogr.* **16**, 132–143.

Griffiths, R. W., Killworth, P. D. & Stern, M. E. 1982 Ageostrophic instability of ocean currents. *J. Fluid Mech.* **117**, 343–377 (referred to herein as GKS).

Houghton, R. W., Schlitz, R., Beardsley, R. C., Butman, B. & Chamberlin, J. L. 1982 The Middle Atlantic Bight cold pool: Evolution of the temperature structure during summer 1979. *J. Phys. Oceanogr.* **12**, 1019–1029.

Johnson, G. L. & Schneider, E. D. 1969 Depositional ridges in the North Atlantic. *Earth Planet. Sci. Lett.* **6**, 416–422.

Killworth, P. D., Paldor, N. & Stern, M. E. 1984 Wave propagation and growth on a surface front in a two-layer geostrophic current. *J. Mar. Res.* **42**, 761–785.

Killworth, P. D. & Stern, M. E. 1982 Instabilities on density-driven boundary currents and fronts. *Geophys. Astrophys. Fluid Dyn.* **22**, 1–28.

LeBlond, P. H. & Mysak, L. A. 1978 *Waves in the Ocean.* Elsevier.

Mory, M., Stern, M. E. & Griffiths, R. W. 1987 Coherent baroclinic eddies on a sloping bottom. *J. Fluid Mech.* **183**, 45–62.

Nof, D. 1983 The translation of isolated cold eddies on a sloping bottom. *Deep-Sea Res.* **30**, 171–182.

Paldor, N. & Killworth, P. D. 1987 Instabilities of a two-layer coupled front. *Deep-Sea Res.* **34**, 1525–1539.

Pedlosky, J. 1987 *Geophysical Fluid Dynamics*, 2nd Edn. Springer.

Smith, P. C. 1976 Baroclinic instability in the Denmark Strait overflow. *J. Phys. Oceanogr.* **6**, 355–371.

Swaters, G. E. & Flierl, G. R. 1991 Dynamics of ventilated coherent cold eddies on a sloping bottom. *J. Fluid Mech.* (in press).

Whitehead, J. A., Stern, M. E., Flierl, G. R. & Klinger, B. A. 1990 Experimental observations of baroclinic eddies on a sloping bottom. *J. Geophys. Res.* **95**, 9585–9610.

Whitehead, J. A. & Worthington, L. U. 1982 The flux and mixing rates of Antarctic Bottom Water within the North Atlantic. *J. Geophys. Res.* **87**, 7903–7924.

Zoccolotti, L. & Salusti, E. 1987 Observations on a very dense marine water in the Southern Adriatic Sea. *Continent. Shelf Res.* **7**, 535–551.